Key Points:
- Horizontal motion of the Earth's surface due to GIA is a result of the interplay of inward mantle flow and the outward moving lithosphere
- Horizontal velocities point inward directly after deglaciation, but start to point outward after a time controlled by mantle viscosity
- Present-day velocities point outward for mantle viscosities below 10^{20} Pa s and inward above 10^{22} Pa s, with a combination in between

Supporting Information:
- Supporting Information S1
- Data Set S1

Correspondence to:
T. H. J. Hermans,
tim.hermans@nioz.nl

Reversal of the Direction of Horizontal Velocities Induced by GIA as a Function of Mantle Viscosity

T. H. J. Hermans[1,2] (iD), W. van der Wal[2,3] (iD), and T. Broerse[3,4] (iD)

[1]Department of Estuarine and Delta Systems, NIOZ Royal Netherlands Institute for Sea Research, and Utrecht University, Yerseke, Netherlands, [2]Faculty of Aerospace Engineering, Delft University of Technology, Delft, Netherlands, [3]Department of Geosciences and Remote Sensing, Delft University of Technology, Delft, Netherlands, [4]Tectonophysics Group, Faculty of Geosciences, Utrecht University, Utrecht, Netherlands

Abstract In regions undergoing glacial isostatic adjustment present-day horizontal surface motion is observed to point mostly, but not always, away from the former ice load. To interpret these observations, we investigate the direction of horizontal velocities using glacial isostatic adjustment models. The direction is controlled by the opposing actions of inward mantle flow and outward lithosphere motion. In contrast with the prevailing idea that glacial isostatic adjustment-induced horizontal velocities point outward, we show that velocities can be either outward or inward. Immediately after deglaciation velocities point inward but change direction to outward after a time that is controlled by mantle viscosity. Present-day horizontal velocities point outward for a uniform mantle viscosity below 10^{20} Pa s and inward for above 10^{22} Pa s, with a combination of outward and inward in between. Our results help to interpret GPS-observed horizontal velocities in areas with varying mantle viscosity.

Plain Language Summary The rebound of the Earth following the disappearance of large ice sheets leads to vertical and horizontal movements of the Earth's surface that can be observed with GPS. To explain GPS observations of postglacial rebound with models, it is important to understand how deformation rates depend on the internal structure of the Earth. Here we investigate how the direction of horizontal velocities depends on the viscosity of the mantle using numerical models. The horizontal velocities result from the opposite movements of different layers inside of the Earth. After melting velocities initially point toward the previously glaciated area, but their direction changes after a time that depends on mantle viscosity. Present-day horizontal velocities at the surface point toward the former ice load for a relatively high mantle viscosity, and point away from the former ice load for relatively low viscosities. Our results show that the direction of horizontal velocities derived from GPS observations can provide important information about the Earth's interior.

1. Introduction

Glacial isostatic adjustment (GIA) is the viscoelastic response of the solid Earth to the growth and retreat of ice sheets and accompanying changes in sea level. Comparing observations of GIA to simulations of forward models can provide information on the deglaciation history and the Earth's rheology. Vertical velocities derived from GPS observations show that formerly ice-covered regions are currently uplifting while surrounding areas (the forebulge) subside. Horizontal velocities often point away from the former ice load (outward) in the previously deglaciated area and just beyond (Kierulf et al., 2014; Milne et al., 2001; Sella et al., 2007). However, an early study by James and Morgan (1990) predicted horizontal velocities pointing toward the former ice sheet (inward) in Hudson Bay, and observed velocities further away from Hudson Bay also point inward (Kreemer et al., 2018; Sella et al., 2007). Furthermore, velocities at sites along the Transantarctic Mountains point toward the presumed former ice load in the Ross Sea Embayment (RSE; Wilson et al., 2015). This could point at the importance of a transition in upper mantle viscosity, which, based on estimates of seismic velocities (e.g., An et al., 2015), is believed to underlie the Transantarctic Mountains. A 3-D viscosity distribution has been shown to affect the pattern of GIA-induced horizontal motion (e.g., Kaufmann et al., 2005; Wu, 2006). However, the dependence of the direction of horizontal velocities on homogeneous mantle viscosity has not been thoroughly analyzed, which makes it difficult to understand how lateral variations in viscosity such as beneath Fennoscandia, the RSE and the Antarctic Peninsula, affect the direction of horizontal motion. For future studies that aim to infer lateral variations in viscosity from

GPS-observed horizontal velocities, it is important to understand the fundamental dependence of the direction of horizontal velocities on homogeneous mantle viscosity.

Using a simple deglaciation history, James and Morgan (1990) found present-day inward horizontal velocities for Hudson Bay, which they explained by the mantle flowing back inward after deglaciation, dragging the lithosphere toward the former ice load. However, outward velocities are predicted with standard GIA models (Milne et al., 2004; Peltier, 1998). Spada et al. (1992) found a combination of outward and inward velocities and attributed differences with respect to the results of James and Morgan (1990) to a different treatment of density discontinuities. James and Lambert (1993) predicted outward velocities for Hudson Bay and the Gulf of Bothnia using the ICE-3G deglaciation model (Tushingham & Peltier, 1991), which were explained by the decreasing flexure of the lithosphere. The difference with the convergent pattern found by James and Morgan (1990) was ascribed to the assumption of incompressibility of the latter. Mitrovica et al. (1994) also predicted outward horizontal velocities beneath the former ice and attributed the difference with the results of James and Morgan (1990) to the assumption of a constant ice disk radius and incompressibility by James and Morgan (1990). Outward velocities were predicted for entire North America by Peltier (1998) and for Fennoscandia by Milne et al. (2004). Sella et al. (2007) found a regionally inward motion in the far field for one of their GIA simulations with increased upper mantle viscosity. However, the prevailing idea, also supported by GPS observations in Fennoscandia (Milne et al., 2001), appears to be that GIA-induced horizontal velocities point outward beneath and directly outside the former ice load.

Horizontal velocities have been shown to be sensitive to lithospheric thickness (e.g., James & Morgan, 1990) and lithospheric rheology (Peltier & Drummond, 2008), mantle structure (O'Keefe & Wu, 2002), lateral viscosity variations (e.g., Kaufmann et al., 2005; King et al., 2016; Wu, 2006), and plate boundaries (Klemann et al., 2008). However, the influence of the magnitude of mantle viscosity on the direction of horizontal velocities through time has not been systematically analyzed. Thus, it is unclear how the direction of observed horizontal motion, which is not purely outward in North America and Antarctica, can constrain GIA models. The aim of this study is to investigate how the direction of GIA-induced horizontal velocities depends on mantle viscosity. We employ a simple loading scenario and an earth model with homogeneous viscosity, allowing us to isolate and explain the effect of mantle viscosity on horizontal velocities before investigating the effect of stratification. We investigate predictions of horizontal velocities for different mantle viscosity and lithospheric thickness values and find that the direction of horizontal motion strongly depends on mantle viscosity. In the supporting information, the effect of mantle stratification and varying ice loads is explored.

2. Methodology

We use a normal mode method (Vermeersen & Sabadini, 1997) to display motion at the Earth's surface through time, and an axisymmetric finite element (FE) model to show internal motion. The FE model was benchmarked against a pseudo-spectral method for radial displacement and geoid anomalies (Wu & van der Wal, 2003). We show in Figure S1 in the supporting information that present-day horizontal velocities between both methods differ only marginally.

2.1. GIA Models

For the FE model, we compute deformation with the commercial software Abaqus (v6.14) following the coupled FE-Laplace approach of Wu (2004). The mesh of the axisymmetric model fills a half-circle with a radius of 6371 km. The model contains 4,320 four-node axisymmetric elements with a width of 0.5° and a depth that varies for each layer (see Table S1 in the supporting information). The spherical harmonic expansion of the gravitational potential is truncated at degree 90. Self-gravitation is computed iteratively in four iterations to ensure convergence to a level below 1%.

The normal mode method produces viscoelastic Love numbers, representing the Earth's response to unit loads (Wu & Peltier, 1982). Here we use a multilayer normal mode method (Vermeersen & Sabadini, 1997). The colatitude resolution and maximum spherical harmonic degree are the same as in the FE model. The Love number computation was benchmarked in Spada et al. (2011), and the combination with surface loads in Martinec et al. (2018).

Ocean loading is not considered as we intend to show only the effect of ice loading. Time steps are defined every 1,000 years during deglaciation and every 2,000 years after. We determine velocities by numerical

differentiation over 100 years around each time step. Degree 1 terms are not included, which results in negligible differences, and the models are incompressible, as compressibility cannot be consistently included in the coupled FE-Laplace approach. Given previous findings of the importance of compressibility for horizontal motion (Mitrovica et al., 1994; Spada et al., 1992; Tanaka et al., 2011), we explore the effects of compressibility (Figure S2 in the supporting information) using a compressible normal mode model (Broerse et al., 2015). The magnitude of the velocities differs and the displacement pattern is more concentrated around the ice margin for a compressible Earth, but the direction agrees with the incompressible results. Predictions of a compressible model can be approximated by adjusting the elastic rigidity of an incompressible model (Tanaka et al., 2011), but since we do not aim to fit observations, we do not pursue this here.

Table S1 in the supporting information provides the elastic structure and density discontinuities of our Earth models, consisting of 12 layers, of which eight have distinctive elastic parameters. The elastic parameters have been obtained by volume-averaging values from the Preliminary Reference Earth Model (Dziewonski & Anderson, 1981). The viscosity of the lithosphere is quasi-infinite, allowing elastic deformation only. The mantle layers deform viscoelastically, with a uniform viscosity that is varied for each test. We vary lithospheric thickness between 50, 90, and 130 km (see Figure S3 in the supporting information).

2.2. Deglaciation History

To study the fundamental dependence of horizontal motion on mantle viscosity, we use an axisymmetric ice cap on the North Pole that is parameterized by

$$h_{\text{ice}}(\phi, t) = H(t) * \frac{\cos(\phi) - \cos(\alpha)}{1 - \cos(\alpha)} \qquad (1)$$

where ϕ is the colatitude, α the colatitude of the ice margin (8°), and H is the ice height at the center of the ice cap (2,200 m). In addition, the load spectrum is tapered above spherical harmonic degree 32 with a cosine filter to reduce the effect of truncation in the spectral domain. The ice cap grows linearly during 90,000 years and reaches its peak height 20,000 years before present (Last Glacial Maximum). It melts linearly during the next 12,000 years until all the ice has disappeared 8,000 years before present. The schematic setup qualitatively represents the ice history of the RSE. The ice load at each time step is applied as a distributed load on the corresponding surface elements. Surface deformation differs for a more realistic deglaciation scenario in which the radius of the ice cap decreases during ice unloading (Mitrovica et al., 1994). However, an ice cap with a radius that decreases 0.5° every 1,000 years of deglaciation results in horizontal velocities that are very similar to the results obtained with a constant radius (see Figure S4a in the supporting information). Increasing ice cap height and radius leads to larger horizontal velocities and a shift in the location of the peak velocity (see Figure S4b in the supporting information).

3. Results and Discussion

3.1. Direction as a Function of Viscosity

We use the axisymmetric FE model to calculate deformation rates for a lithospheric thickness of 90 km and uniform mantle viscosity (η) that is varied from 10^{19} to 10^{23} Pa s with steps of one order of magnitude. Figure 1 shows the present-day horizontal velocities for these and two intermediate steps. The horizontal velocity $\dot{v}$ is defined positive for outward velocities and negative for inward velocities.

Figure 1 clearly shows that the direction of horizontal velocities is controlled by mantle viscosity. For $\eta = 10^{20}$ Pa s, horizontal velocities point outward over a large distance from the ice center, whereas for $\eta = 10^{22}$ Pa s, horizontal velocities point inward. For $\eta = 10^{21}$ Pa s, there is a sharp alternation of outward and inward direction. We will show in section 3.3 that this is the result of the sloped lithosphere that is flexing back to its horizontal equilibrium position. Thus, the direction of present-day horizontal velocities can reverse depending on mantle viscosity. Further varying mantle viscosity with steps of tenths of an order of magnitude, we find that outward motion in the near field is bounded by $\eta \leq 2 \times 10^{20}$ Pa s and inward motion by $\eta \geq 4 \times 10^{21}$ Pa s (dashed curves in Figure 1), with a combination in between. In the following section we will investigate how mantle viscosity can result in a reversed direction by studying how horizontal motion varies with depth.
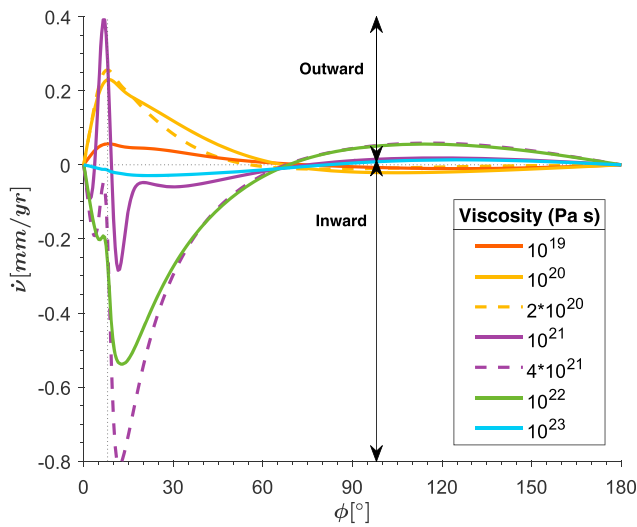
Figure 1. Present-day horizontal velocities ($\dot{v}$) as a function of colatitude ϕ for varying mantle viscosity as a result of the growth and melt of an axisymmetric ice cap with a radius of 8° (dashed vertical line) centered at the North Pole.

3.2. Opposite Motions in Mantle and Lithosphere

To follow horizontal motion through time, Figure 2 shows velocities at FE nodes at the surface and at deeper layer boundaries during ice melt and at present day in a cross-sectional view of the Earth. Additionally, the shear stress $\sigma_{r\theta}$ on elements at the bottom of the lithosphere is shown, which at the bottom of an element is defined negative in the tangential direction. Velocities and stress are plotted for $\eta = 10^{20}$ Pa s, for which velocities point outward at present day, and $\eta = 10^{22}$ Pa s, for which velocities point inward (see Figure 1).

For both mantle viscosities, the model predicts a strong inward and upward motion of the mantle during deglaciation (Figures 2a and 2b). This can be understood by mantle material flowing back to the ice center after it was pushed downward and outward during ice loading (James & Morgan, 1990; O'Keefe & Wu, 2002). For $\eta = 10^{22}$ Pa s, velocities are smaller due to the slower relaxation of a more viscous mantle. The elastic lithosphere is flexing upward during deglaciation and relaxation (James & Lambert, 1993). While flexing upward, the part of the lithosphere that was sloped downward becomes horizontal, which is only possible if the lithosphere moves outward. Thus, the mantle and the lithosphere move in opposite directions during deglaciation and relaxation, as was found by O'Keefe and Wu (2002). However, Figures 2a and 2b show that both
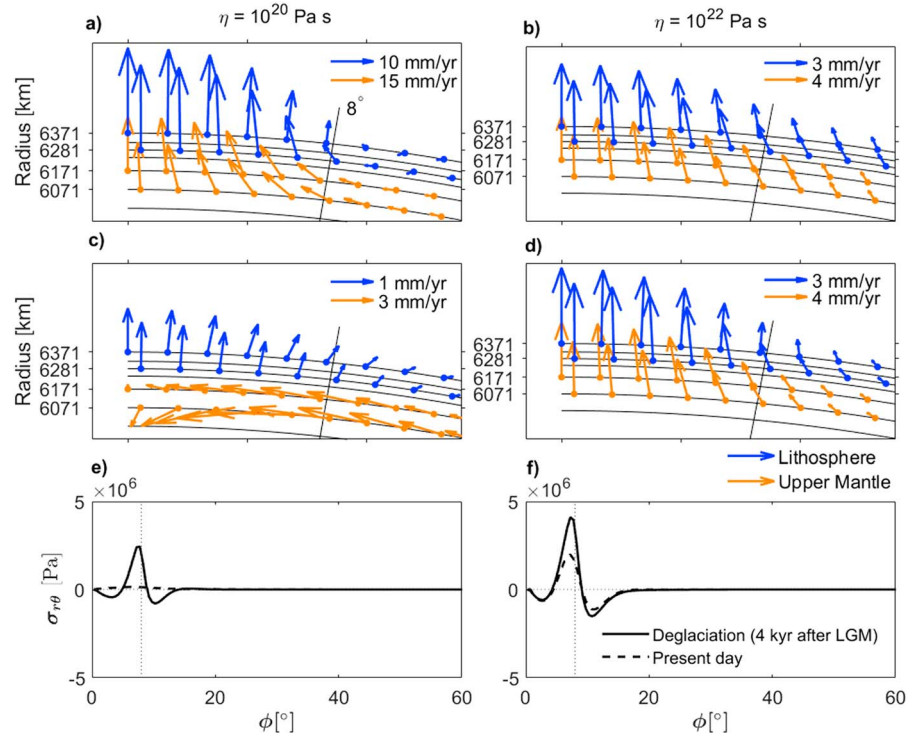

Figure 2. Velocities of nodes on layer boundaries in the lithosphere (blue arrows) and upper mantle (orange arrows) in a cross-sectional view of the Earth, during deglaciation (4,000 years after the Last Glacial Maximum) for (a) $\eta = 10^{20}$ Pa s and (b) $\eta = 10^{22}$ Pa s, at present day (8,000 years after melting ended) for (c) $\eta = 10^{20}$ Pa s and (d) $\eta = 10^{22}$ Pa s, and shear stress at the bottom of the lithosphere during deglaciation and at present day for (e) $\eta = 10^{20}$ Pa s and (f) $\eta = 10^{22}$ Pa s. Note the different scales for the lithospheric and upper mantle velocities in each panel.

the mantle and the lithosphere move inward during deglaciation. From that, it follows that the inward mantle flow dominates over the outward motion of the lithosphere, causing horizontal surface velocities to point inward. During deglaciation, for both mantle viscosities, the shear stress at the bottom of the lithosphere (Figures 2e and 2f) is negative outside of the forebulge as a result of outward mantle flow during ice loading, and positive near the forebulge due to the flexure of the lithosphere.

At present day, the direction of horizontal motion differs substantially for the two different mantle viscosities (Figures 2c and 2d). For $\eta = 10^{22}$ Pa s, horizontal velocities in the mantle and the lithosphere point inward like during deglaciation. For $\eta = 10^{20}$ Pa s, the horizontal surface velocities point outward while the mantle continues to flow inward, driving upward surface motion and even downward motion of deeper layers. For $\eta = 10^{22}$ Pa s, present-day shear stress at the bottom of the lithosphere is reduced due to inward mantle flow but is still significantly negative outside of the forebulge and positive near the forebulge, indicating that the lithosphere is still flexed. For $\eta = 10^{20}$ Pa s, the shear stress is significantly reduced at all colatitudes and is slightly positive, indicating that the mantle has flown inward and the lithosphere has moved toward its horizontal equilibrium position (Figures 2e and 2f). The resulting outward surface motion now dominates the inward mantle flow, which is why the direction of horizontal velocities changes after deglaciation. Nevertheless, the inward mantle flow continues at present day. The rate of change of the horizontal gravity component derived from GRACE data, which points toward the former ice load, confirms this (van der Wal et al., 2011). For $\eta = 10^{22}$ Pa s, this stage of relaxation has not yet been reached, which is why velocities still point inward at present day. The next section investigates how the direction changes with time during relaxation.

3.3. Time-Dependent Change of Direction

We now focus on the time-dependent behavior of horizontal velocities during relaxation for mantle viscosities of 10^{20} and 10^{22} Pa s. To isolate relaxation, we use the normal mode method to predict velocities after a Heaviside loading with the same dimensions as the ice load described in section 2.2. We place the ice load on the surface for 10 Myr (billion years for $\eta = 10^{22}$ Pa s) to reach equilibrium, and then remove it instantaneously, after which the Earth relaxes freely. Figure 3 shows vertical displacement (u), horizontal displacement (v), and $\dot{\mathbf{v}}$ at various time steps.

The initial vertical displacement in Figures 3a and 3b shows a depression underneath the ice cap and a forebulge outside the ice margin. The lithosphere is sloped between the center of the former ice cap and the forebulge with the maximum slope at 7° colatitude. Figures 3c and 3d show that for both mantle viscosities, the horizontal displacement at $t = 0$ is positive because the mantle flowed outward during ice loading. A local minimum in outward horizontal displacement at $t = 0$ can be found at 7°, where the lithosphere has its maximum slope. Following the removal of the load, for both viscosities, the initial outward displacement is reduced by inward mantle flow. However, for $\eta = 10^{20}$ Pa s, the inward movement of the surface reverses markedly after around 0.8 kyr, when the forebulge subsides and the slope of the lithosphere reduces, pushing the surface outward. This can be seen more clearly in Figure 4, which shows the displacement through time for at 7° and 9° colatitude. The time of reversal is determined by the characteristic time scale of relaxation of the mantle, which is a function of mantle viscosity. Hence, the displacement at 16 kyr for a $\eta = 10^{22}$ Pa s equals the displacement at 160 years for $\eta = 10^{20}$ Pa s. For $\eta = 10^{22}$ Pa s, the lithosphere is still sloped and surface movement remains inward.

At 9° colatitude (Figure 4b), the uplift rate is initially positive, indicating that the forebulge increases in height before it starts to subside around $t = 0.4$ kyr for $\eta = 10^{20}$ Pa s. The subsidence is not yet seen at that time for $\eta = 10^{22}$ Pa s. When the forebulge has almost completely subsided, the direction of the horizontal displacement reverses. Thus, the collapse of the forebulge seems to enable the sloped lithosphere to return to a horizontal position, causing horizontal velocities to point outward. The trend in displacement reverses earlier at 7° colatitude, as here the slope of the lithosphere is the largest. The displacement for $\eta = 10^{22}$ Pa s follows the same path but slower. Therefore, the reversal in direction is not seen even 16 kyr after deglaciation.

Figure 3e indeed shows that for $\eta = 10^{20}$ Pa s, horizontal surface velocities are negative until the moment of forebulge collapse, and are positive afterward. For $\eta = 10^{22}$ Pa s, horizontal velocities remain negative for the period under consideration because of the slower relaxation (Figure 3f). A mantle viscosity of 10^{21} Pa s presents an intermediate case in which the forebulge is subsiding at present day but has not yet completely
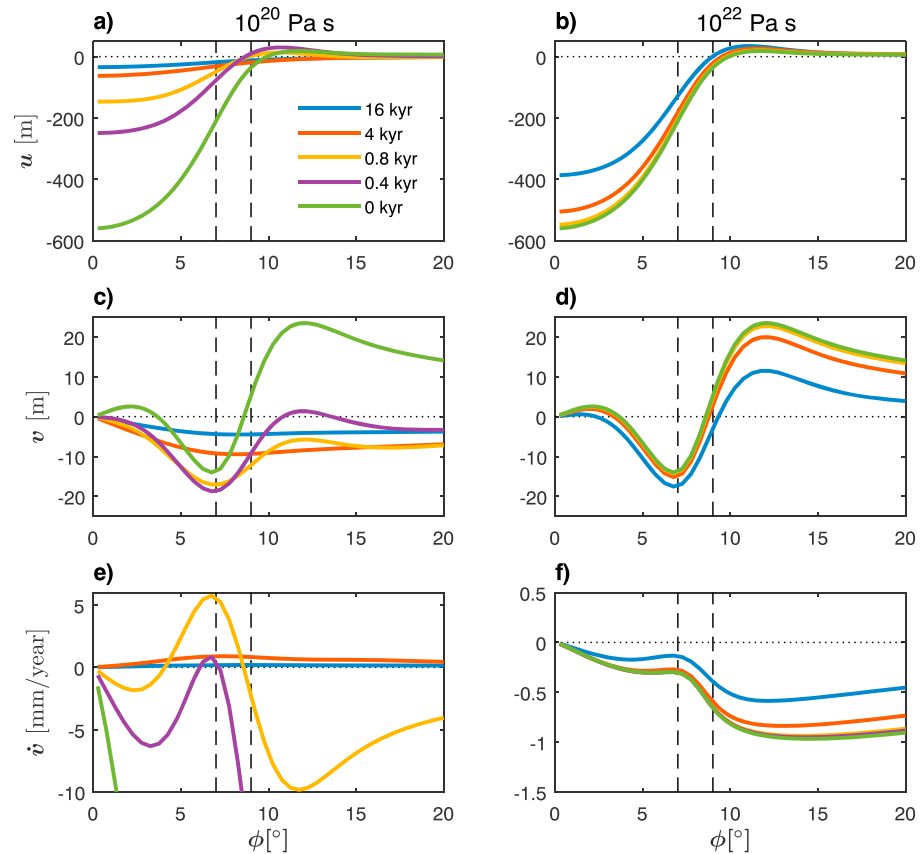
Figure 3. Vertical and horizontal displacement u and v as a function of colatitude ϕ for (a and c) $\eta = 10^{20}$ Pa s and (b and d) 10^{22} Pa s and horizontal velocities $\dot{v}$ for (e) $\eta = 10^{20}$ Pa s and (f) 10^{22} Pa s. The dashed vertical lines indicate 7° and 9° colatitude for which displacement is shown in Figure 4.
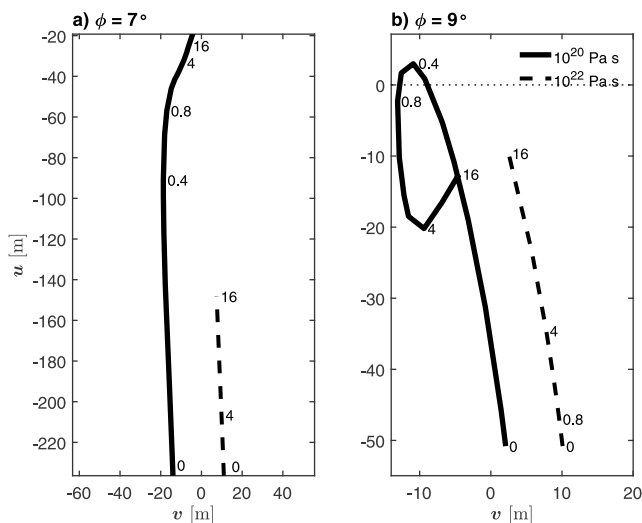

Figure 4. Horizontal and vertical displacement of the surface at (a) 7° and (b) 9° colatitude for both viscosities. For visibility, the curve for $\eta = 10^{22}$ Pa s has been displaced horizontally by 25 m in (a) and 8 m in (b). Labels denote the time in kyr after removing the ice cap.

collapsed. Thus, the lithosphere is in the process of returning from a sloped to a horizontal position, which causes inward horizontal velocities for $\eta = 10^{21}$ Pa s to start pointing outward at 7° colatitude (Figure 4). This explains the horizontal velocities for $\eta = 10^{21}$ Pa s in Figure 1, which are positive around 7° colatitude and negative elsewhere.

The reversal of the direction of horizontal velocities also occurs for Earth models with a lithospheric thickness of 50 and 130 km (see Figure S3 in the supporting information). However, the influence of inward mantle flow on horizontal surface velocities is stronger for a thinner lithosphere (Mitrovica et al., 1994). As a result, the exact mantle viscosities that bound the reversal of present-day outward to inward motion decrease for a lithosphere thickness of 50 km ($\eta \leq 10^{20}$ and $\eta \geq 10^{21}$ Pa s) and increase for a lithosphere thickness of 130 km ($\eta \leq 5 \times 10^{20}$ and $\eta \geq 2 \times 10^{22}$ Pa s).

A consistent finding in GIA studies is that mantle viscosity increases from upper to lower mantle (e.g., Lau et al., 2016; Peltier, 2004). Therefore, we also test the effect of increased lower mantle viscosity. As mantle flow is confined to the upper mantle, which has lower viscosity, we find that for an increase in lower mantle viscosity by a factor of 10, the magnitude of present-day horizontal velocities at the surface increases, in agreement with Mitrovica et al. (1994). The reversal in direction is less sensitive to stratification: the upper mantle viscosities that bound outward and inward

motion deviate only by a factor 1.5 or less from the solution of the homogeneous case (see Figure S5 in the supporting information).

4. Conclusions

In contrast with the prevailing idea of GIA-induced horizontal velocities pointing outward in previously glaciated regions, we show that present-day horizontal velocities either point outward or inward, as a function of mantle viscosity. By studying modeled velocities in the lithosphere and the upper mantle, we show that the dependence of direction on viscosity is a result of the opposing motions of inward mantle flow and the lithosphere that moves outward while returning from a flexed to a horizontal position. After deglaciation, velocities at the surface first point inward but change direction after a time determined by mantle viscosity. For all variations of lithospheric thickness that were included, this results in present-day horizontal velocities that in the near field all point outward for $\eta < 10^{20}$ Pa s, inward for $\eta > 10^{22}$ Pa s, and in a combination of inward and outward velocities in between. The exact mantle viscosities for which present-day direction reverses depend on lithospheric thickness, and are only slightly affected by stratification of viscosity.

The results of this study show that the direction of the velocities places a strong constraint on upper mantle viscosity when time since deglaciation is approximately known. Whenever consistent outward motion is observed, viscosities beneath the former Last Glacial Maximum ice load must be below 10^{21} Pa s. This is the case in Fennoscandia (Milne et al., 2001). Velocities in North America show outward motion but there is also evidence for inward motion further away from the area of former deglaciation (Kreemer et al., 2018; Sella et al., 2007). This agrees with the situation of $\eta = 10^{21}$ Pa s in Figures 1 and S5. Our study also forms a basis to understand predictions of 3-D GIA models. Horizontal motion predicted by such models is described as directed from a high-viscosity region toward a low-viscosity region (Kaufmann et al., 2005). Our study suggests that it may be the unfinished relaxation in a high-viscosity region that leads to velocities that point toward the former ice load in 3-D models.

Velocities that point toward the presumed location of former ice load are observed in a region west of the RSE where a lateral transition is expected from low mantle viscosity underneath the RSE to high mantle viscosity underneath East Antarctica (Wilson et al., 2015). Our study suggests that high mantle viscosity could indeed explain the observed inward motion. An alternative reason could be more recent ice unloading (Figure 3). Thus, velocities that point toward the former ice load can provide an important and rare constraint on mantle viscosity and potentially on lateral changes in mantle viscosity. This motivates future investigation of GPS velocities to constrain expected lateral viscosity transitions in regions such as Antarctica, Patagonia, and Alaska.

References

An, M., Wiens, D. A., Zhao, Y., Feng, M., Nyblade, A. A., Kanao, M., et al. (2015). S-velocity model and inferred Moho topography beneath the Antarctic plate from Rayleigh waves. *Journal of Geophysical Research: Solid Earth*, *120*, 359–383. https://doi.org/10.1002/2014JB011332

Broerse, T., Riva, R. E. M., Simons, W., Govers, R., & Vermeersen, L. L. A. (2015). Postseismic GRACE and GPS observations indicate a rheology contrast above and below the Sumatra slab. *Journal of Geophysical Research: Solid Earth*, *120*, 5343–5361. https://doi.org/10.1002/2015JB011951

Dziewonski, A. M., & Anderson, D. L. (1981). Preliminary reference earth model. *Physics of the Earth and Planetary Interiors*, *25*(4), 297–356. https://doi.org/10.1016/0031-9201(81)90046-7

James, T. S., & Lambert, A. (1993). A comparison of VLBI data with the ICE-3G glacial rebound model. *Geophysical Research Letters*, *20*(9), 871–874. https://doi.org/10.1029/93GL00865

James, T. S., & Morgan, W. J. (1990). Horizontal motions due to post-glacial rebound. *Geophysical Research Letters*, *17*(7), 957–960. https://doi.org/10.1029/GL017i007p00957

Kaufmann, G., Wu, P., & Ivins, E. R. (2005). Lateral viscosity variations beneath Antarctica and their implications on regional rebound motions and seismotectonics. *Journal of Geodynamics*, *39*(2), 165–181. https://doi.org/10.1016/j.jog.2004.08.009

Kierulf, H. P., Steffen, H., Simpson, M. J. R., Lidberg, M., Wu, P., & Wang, H. (2014). A GPS velocity field for Fennoscandia and a consistent comparison to glacial isostatic adjustment. *Journal of Geophysical Research: Solid Earth*, *119*, 6613–6629. https://doi.org/10.1002/2013JB010889

King, M. A., Whitehouse, P. L., & van der Wal, W. (2016). Incomplete separability of Antarctic plate rotation from glacial isostatic adjustment deformation within geodetic observations. *Geophysical Journal International*, *204*(1), 324–330. https://doi.org/10.1093/gji/ggv461

Klemann, V., Martinec, Z., & Ivins, E. R. (2008). Glacial isostasy and plate motion. *Journal of Geodynamics*, *46*(3-5), 95–103. https://doi.org/10.1016/j.jog.2008.04.005

Kreemer, C., Hammond, W. C., & Blewitt, G. (2018). A robust estimation of the 3-D intraplate deformation of the North American plate from GPS. *Journal of Geophysical Research: Solid Earth*, *123*, 4388–4412. https://doi.org/10.1029/2017JB015257

Lau, H. C., Mitrovica, J. X., Austermann, J., Crawford, O., Al-Attar, D., & Latychev, K. (2016). Inferences of mantle viscosity based on ice age data sets: Radial structure. *Journal of Geophysical Research: Solid Earth*, *121*, 6991–7012. https://doi.org/10.1002/2016JB013043

Martinec, Z., Klemann, V., van der Wal, W., Riva, R. E. M., Spada, G., Sun, Y., et al. (2018). A benchmark study of numerical implementations of the sea level equation in GIA modelling. *Geophysical Journal International*, *215*(1), 389–414. https://doi.org/10.1093/gji/ggy280

Milne, G. A., Davis, J. L., Mitrovica, J. X., Scherneck, H. G., Johansson, J. M., Vermeer, M., & Koivula, H. (2001). Space-geodetic constraints on glacial isostatic adjustment in Fennoscandia. *Science*, *291*(5512), 2381–2385. https://doi.org/10.1126/science.1057022

Milne, G. A., Mitrovica, J. X., Scherneck, H. G., Davis, J. L., Johansson, J. M., Koivula, H., & Vermeer, M. (2004). Continuous GPS measurements of postglacial adjustment in Fennoscandia: 2. Modeling results. *Journal of Geophysical Research*, *109*, B02412. https://doi.org/10.1029/2003JB002619

Mitrovica, J. X., Davis, J. L., & Shapiro, I. I. (1994). A spectral formalism for computing three-dimensional deformations due to surface loads 2. Present-day glacial isostatic adjustment. *Journal of Geophysical Research*, *99*(B4), 7075–7101. https://doi.org/10.1029/93JB03401

O'Keefe, K., & Wu, P. (2002). Effect of mantle structure on postglacial induced horizontal displacement. In J. X. Mitrovica, & L. L. A. Vermeersen (Eds.), *Ice Sheets, Sea Level and the Dynamic Earth, Geodynamics Series 29* (pp. 109–118). Washington: American Geophysical Union. https://doi.org/10.1002/9781118670101.ch7

Peltier, W. R. (1998). Postglacial variations in the level of the sea: Implications for climate dynamics and solid-Earth geophysics. *Reviews of Geophysics*, *36*(4), 603–689. https://doi.org/10.1029/98RG02638

Peltier, W. R. (2004). Global glacial isostasy and the surface of the ICE-age earth: The ICE-5G (VM2) model and GRACE. *Annual Review of Earth and Planetary Sciences*, *32*(1), 111–149. https://doi.org/10.1146/annurev.earth.32.082503.144359

Peltier, W. R., & Drummond, R. (2008). Rheological stratification of the lithosphere: A direct interference based upon the geodetically observed pattern of glacial isostatic adjustment of the north American continent. *Geophysical Research Letters*, *35*, L16314. https://doi.org/10.1029/2008GL034586

Sella, G. F., Stein, S., Dixon, T. H., Craymer, M., James, T. S., Mazzotti, S., & Dokka, R. K. (2007). Observation of glacial isostatic adjustment in stable North America with GPS. *Geophysical Research Letters*, *34*, L02306. https://doi.org/10.1029/2006GL027081

Spada, G., Barletta, V. R., Klemann, V., Riva, R. E. M., Martinec, Z., Gasperini, P., et al. (2011). A benchmark study for glacial isostatic adjustment codes. *Geophysical Journal International*, *185*(1), 106–132. https://doi.org/10.1111/j.1365-246X.2011.04952.x

Spada, G., Sabadini, R., Yuen, D. A., & Ricard, Y. (1992). Effects on post-glacial rebound from the hard rheology in the transition zone. *Geophysical Journal International*, *109*(3), 683–700. https://doi.org/10.1111/j.1365-246X.1992.tb00125.x

Tanaka, Y., Klemann, V., Martinec, Z., & Riva, R. E. M. (2011). Spectral-finite element approach to viscoelastic relaxation in a spherical compressible Earth: Application to GIA modelling. *Geophysical Journal International*, *184*(1), 220–234. https://doi.org/10.1111/j.1365-246X.2010.04854.x

Tushingham, A. M., & Peltier, W. R. (1991). Ice-3G: A new global model of late Pleistocene deglaciation based upon geophysical predictions of post-glacial relative sea level change. *Journal of Geophysical Research*, *96*(B3), 4497–4523. https://doi.org/10.1029/90JB01583

van der Wal, W., Kurtenbach, E., Kusche, J., & Vermeersen, L. L. A. (2011). Radial and tangential gravity rates from GRACE in areas of glacial isostatic adjustment. *Geophysical Journal International*, *187*(2), 797–812. https://doi.org/10.1111/j.1365-246X.2011.05206.x

Vermeersen, L. L. A., & Sabadini, R. (1997). A new class of stratified viscoelastic models by analytical techniques. *Geophysical Journal International*, *129*(3), 531–570. https://doi.org/10.1111/j.1365-246X.1997.tb04492.x

Wilson, T. J., Bevis, M. G., Konfal, S. A., Barletta, V. R., Aster, R. C., Chapot, J., et al. (2015). Understanding glacial isostatic adjustment and ice mass change in Antarctica using integrated GPS and seismology observations. Geophysical Research Abstracts, 17, EGU2015.

Wu, P. (2004). Using commercial finite element packages for the study of Earth deformations, sea levels and the state of stress. *Geophysical Journal International*, *158*(2), 401–408. https://doi.org/10.1111/j.1365-246X.2004.02338.x

Wu, P. (2006). Sensitivity of relative sea levels and crustal velocities in Laurentide to radial and lateral viscosity variations in the mantle. *Geophysical Journal International*, *165*(2), 401–413. https://doi.org/10.1111/j.1365-246X.2006.02960.x

Wu, P., & Peltier, W. R. (1982). Viscous gravitational relaxation. *Geophysical Journal International*, *70*(2), 435–485. https://doi.org/10.1111/j.1365-246X.1982.tb04976.x

Wu, P., & van der Wal, W. (2003). Postglacial sea levels on a spherical, self-gravitating viscoelastic earth: Effects of lateral viscosity variations in the upper mantle on the inference of viscosity contrasts in the lower mantle. *Earth and Planetary Science Letters*, *211*(1–2), 57–68. https://doi.org/10.1016/S0012-821X(03)00199-7

Erratum

In the originally published version of this article, Figure 2e was published incorrectly. This error has since been corrected, and this version may be considered the authoritative version of record.